Applied Surface Science 508 (2020) 144937

Contents lists available at ScienceDirect

Applied Surface Science

journal homepage: www.elsevier.com/locate/apsusc

Full Length Article

Vanadium dopant- and strain-dependent magnetic properties of single-layer VI_3

M. Baskurt[a], I. Eren[b], M. Yagmurcukardes[c,*], H. Sahin[a,d]

[a] Department of Photonics, Izmir Institute of Technology, 35430 Izmir, Turkey
[b] Department of Physics, Izmir Institute of Technology, 35430 Izmir, Turkey
[c] Department of Physics, University of Antwerp, Groenenborgerlaan 171, B-2020 Antwerp, Belgium
[d] ICTP-ECAR Eurasian Center for Advanced Research, Izmir Institute of Technology, 35430 Izmir, Turkey

A B S T R A C T

Motivated by the recent synthesis of two-dimensional VI_3 [Kong et al. Adv. Mater. **31**, 1808074 (2019)], we investigate the effect of V doping on the magnetic and electronic properties of monolayer VI_3 by means of first-principles calculations. The dynamically stable semiconducting ferromagnetic (FM) and antiferromagnetic (AFM) phases of monolayer VI_3 are found to display distinctive vibrational features that the magnetic state can be distinguished by Raman spectroscopy. In order to clarify the effect of experimentally observed excessive V atoms, the magnetic and electronic properties of the V-doped VI_3 structures are analyzed. Our findings indicate that partially doped VI_3 structures display FM ground state while the fully-doped structure exhibits AFM ground state. The fully-doped monolayer VI_3 is found to be a semiconductor with a relatively larger band gap than its pristine structure. In addition, strain-dependent electronic and magnetic properties of fully- and partially-doped VI_3 structures reveal that pristine monolayer displays a FM-to-AFM phase transition with robust semiconducting nature for 5% of compressive strain, while fully-doped monolayer VI_3 structure possesses AFM-to-FM semiconducting transition at tensile strains larger than 4%. In contrast, the partially-doped VI_3 monolayers are found to display robust FM ground state under biaxial strain. Its dopant and strain tunable electronic and magnetic nature makes monolayer VI_3 a promising material for applications in nanoscale spintronic devices.

1. Introduction

Searching for magnetism at two-dimensional (2D) limit has been the focus of interest over the past two decades since the discovery of graphene [1]. Although, graphene and other synthesized 2D materials were announced to be non-magnetic, magnetism was shown to exist in case of introducing edges by cutting the material to a nanoribbon [2–4], by adatoms [5,6], or by the presence of vacancies [7].

Even though layered magnetic van der Waals (vdW) crystals have been known for a long time [8–10], recent experimental achievements on their exfoliation to monolayer limit made 2D magnetic materials important candidates for nanoscale spintronic applications [11–13]. Recently synthesized monolayers of semiconducting ferromagnets, CrI_3 [14] and $Cr_2Ge_2Te_6$ [15], have increased the attention on 2D magnetic materials [16]. In addition, monolayer CrI_3 was reported to exhibit tunable magnetism between FM and AFM phases by either application of an external electric field [17] or magnetic field [18,19]. Moreover, recently other novel 2D magnetic monolayers such as $RuCl_3$ [20,21], VSe_2 [22,23], $MnSe_2$ [24], $FeCl_2$ [25], and VCl_3 [26], have been added to library of 2D magnetic materials.

Magnetic layered vdW crystal of VI_3 was studied long before the 2D magnetic materials were discovered [27,28]. In recent studies, VI_3 was reported to exhibit promising structural, magnetic and electronic properties similar to CrI_3 [29,30]. Very recently, 2D form of VI_3 was successfully isolated as a FM semiconductor [31]. It was demonstrated that VI_3 undergoes structural and magnetic phase transitions at 78 and 49 K, respectively. In addition, it was observed that through the synthesis process, VI_3 forms with excessive doping of V atoms. It has been investigated in many 2D materials that dopants or vacancies can alter the electronic and magnetic properties of 2D crystals [32] and may lead to anisotropy in the structure [33].

Motivated by the recent results on 2D VI_3,[31] in this study, we investigate and clarify the effect of experimentally observed excessive V atoms on the electronic and magnetic properties of dynamically stable monolayer VI_3. Our results reveal that FM ground state and AFM states of VI_3 exhibit distinctive features in their Raman spectra which allows one to distinguish the magnetic state. In addition, we show that increasing the V dopant level in VI_3 leads to the magnetic phase transition from FM-to-AFM as the structure is fully-doped. Furthermore, the pristine and fully-doped VI_3 structures are shown to display phononic stability in the range of ±5% biaxial strain with tunable electronic or magnetic properties. The paper is organized as follows: Details of the computational methodology are given in Section 2. Results on the structural, vibrational, and electronic properties of FM and AFM phases

* Corresponding author.
E-mail address: Mehmet.Yagmurcukardes@uantwerpen.be (M. Yagmurcukardes).

https://doi.org/10.1016/j.apsusc.2019.144937
Received 18 September 2019; Received in revised form 14 November 2019; Accepted 3 December 2019
Available online 24 December 2019

of VI_3 are presented and the effects of different concentrations of excessive V atoms on electronic and magnetic properties of VI_3 are discussed in Section 3. Magnetic and electronic responses of pristine and doped VI_3 structures to the applied biaxial strain are discussed in Section 4. Results are concluded in Section 5.

2. Computational methodology

The structural optimizations, magnetic, electronic, and vibrational properties of the monolayer VI_3 and its V-doped structures were carried out by means of the first-principles calculations within the density functional theory (DFT) as implemented in Vienna *ab initio* Simulation Package (VASP) [34,35]. Projector augmented-wave (PAW)[36] potentials were used, for V atom 2 electrons in *s*-orbital and 3 electrons in *d*-orbital, total of 5 valence electrons were treated by the PAW potential. The exchange-correlation functionals were adapted by generalized gradient approximation (GGA) of Perdew-Burke-Ernzerhof (PBE) [37]. The van der Waals correction was implemented by the DFT-D3 method with Becke-Jonson damping [38]. The charge transfer between the individual atoms was determined by the Bader technique [39].

The convergence criteria for the total energy difference between consequent steps was taken as 10^{-5} eV. The kinetic energy cutoff of the plane-wave basis set was 250 eV in all calculations. Fermi level broadening was done by Gaussian smearing by using a broadening width of 0.05 eV was chosen for geometry optimizations. At least 15 Å of vacuum space was inserted in order to prevent any unphysical interactions between the layers repeated in the out-of-plane direction. Geometry optimizations of the crystals were allowed until pressures in all directions are less than 1 kB. The phonon modes both at the Γ point and in the whole Brillouin zone (BZ) were calculated by using the small displacement method as implemented in the PHON and PHONOPY codes [40,41], and the corresponding off-resonant Raman activities were obtained from the derivative of dielectric constant [42,43].

3. Results

In its primitive unitcell, monolayer VI_3 consists of 2-V and 6-I atoms where each V atom forms VI_6 octahedron with I atoms. As shown in Fig. 1(a) and (b), the edge-shared VI_6 octahedrons form a honeycomb network of V atoms with the space group of $R\bar{3}$ similar to the crystal structure of monolayer CrI_3 [44,46]. Crystal structure of VI_3 displays slight structural differences in FM and AFM phases. As listed in Table 1, the lattice parameters are calculated to be 6.85 Å and 6.75 Å for the FM and AFM phases, respectively. V-I bond length is found to be 2.74 Å in FM phase, however, it is found to have three different values (2.69 Å, 2.74 Å, and 2.78 Å) in AFM state. Similarly, V-V atomic distance in FM phase is found to be 3.96 Å while in AFM phase two values are found, 3.60 Å between the V atoms with the same spin orientation and 4.05 Å for those having opposite spin orientations. According to the Bader charge analysis, each V atom donates 1.1 e^- to six I atoms in both magnetic phases. Total energy differences are calculated for both magnetic phases and FM phase is found to be energetically favorable. Cohesive energies of FM and AFM phases are calculated to be 3.08 eV and 3.07 eV per atom, respectively. In addition, work function of FM and AFM phases are found to be 5.23 eV and 5.18 eV, respectively. Compare to the work function of 2D magnetic semiconductor CrI_3, which is reported to be 5.35 eV [45], VI_3 has lower work function.

Dynamical stability of monolayer VI_3 for two different magnetic states is investigated by calculating their phonon band dispersions through the whole BZ and are shown in Fig. 1(c) and (d). The phonon branches are found to be free from any imaginary frequencies indicating the dynamical stability of monolayer VI_3 at both FM and AFM states, respectively. Apparently, magnetic state of the structure can also be monitored via phonon band dispersions. Phonon frequencies and corresponding eigenfunctions are obtained at the Γ point in order to calculate the first-order off-resonant Raman spectrum for both magnetic states. The Raman spectrum calculations reveal that both FM and AFM monolayer VI_3 exhibit seven prominent Raman active modes which are shown below Fig. 1(e).

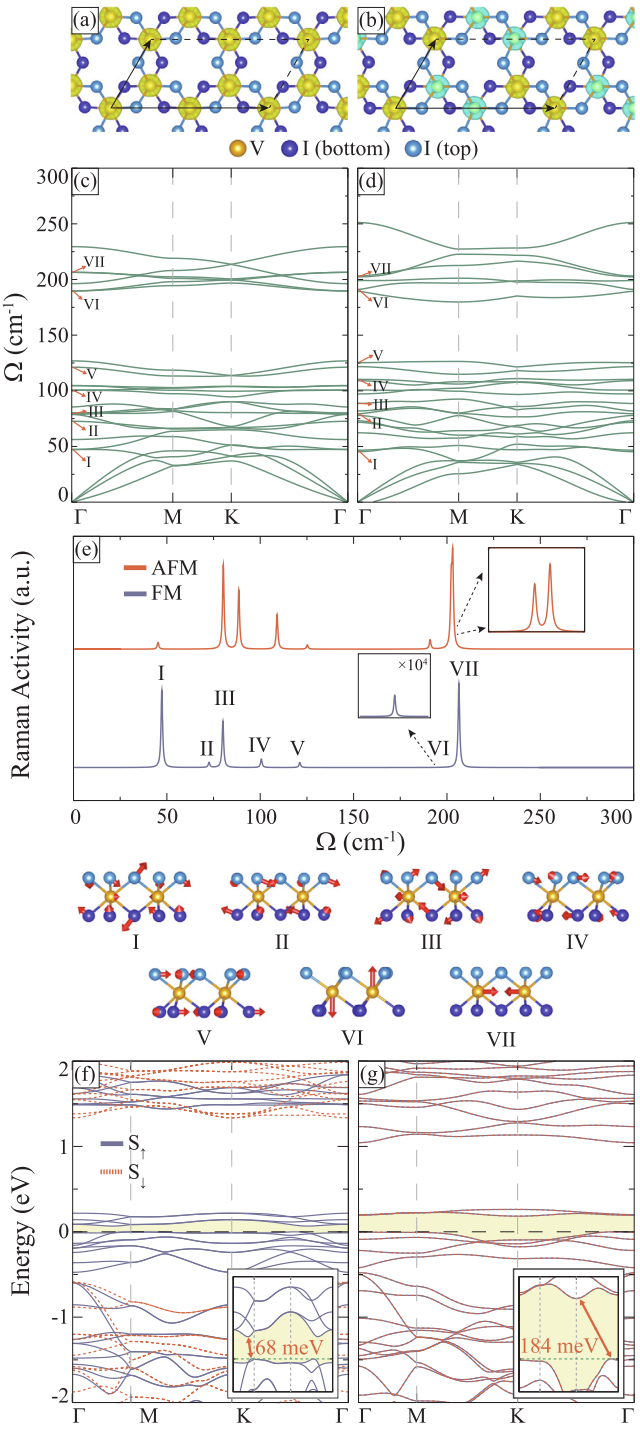

Fig. 1. For the FM and AFM states of monolayer VI_3; (a, b) top view of the 2 × 1 supercell structure with charge density differences, (c, d) the phonon band dispersions, (e) corresponding Raman spectra with the vibrational character of prominent Raman active modes, and (f, g) electronic band dispersions. The insets show the band dispersions around the Fermi level which is set to zero. Up and down spin components are denoted by blue and red lines, respectively. Yellow and blue colors represent up and down magnetic moment, respectively. The isosurface level of charge density difference is set to 0.02 eV/Å^3. (For interpretation of the references to colour in this figure legend, the reader is referred to the web version of this article.)

In order to compare the Raman active modes of both magnetic

Table 1
Calculated parameters for AFM and FM phases of VI_3: magnetic state, optimized lattice constants, $a = b$; distance between V-I, d_{V-I}; and V-V atoms, d_{V-V}; total magnetic moment per primitive cell, μ; total amount of electron received per I atom, ρ_I; cohesive energy per atom, E_{Coh}; total energy difference per atom with respect to the ground state energy, ΔE; work function, Φ; and the energy band gap calculated within GGA, E_{gap}^{GGA}.

Magnetic state	$a = b$ (Å)	d_{V-I} (Å)	d_{V-V} (Å)	μ (μ_B)	ρ_I (e^-)	E_{Coh} (eV)	ΔE (meV)	Φ (eV)	E_{gap}^{GGA} (meV)
FM	6.85	2.74	3.96	4	0.4	3.084	0	5.23	68
AFM	6.75	2.69–2.74–2.78	3.60–4.06	0	0.4	3.073	11	5.18	184

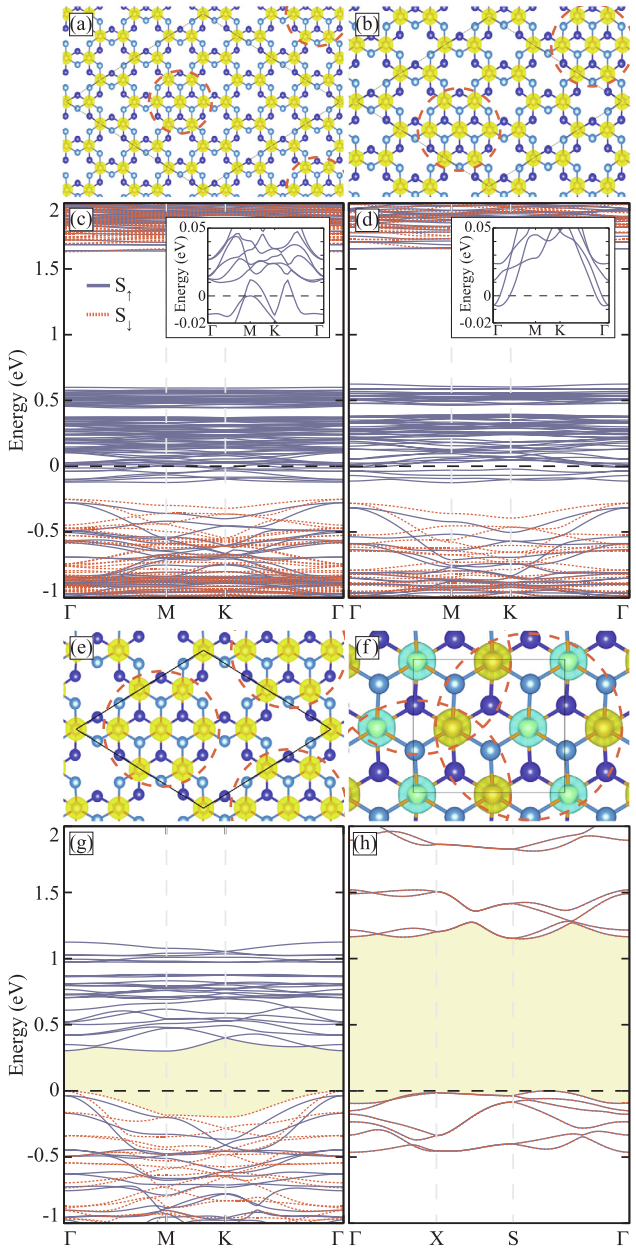

Fig. 2. (a,b) and (e,f) The spin polarized charge density differences (isosurface level is set to 0.02 eV/Å^3) for 1/16, 1/9, 1/4, and fully-doped VI_3, respectively. (c,d) and (g,h) The corresponding electronic band dispersions, respectively. V doped regions are highlighted by red-dashed circles.

phases, phonon modes are labeled from I-to-VII as given in the inset of Fig. 1(e). The highest frequency optical modes, labeled as VI and VII, arise from the pure opposite out-of-plane and in-plane vibrations of V atoms, respectively. The phonon mode-VII is doubly-degenerate for FM state while a small splitting of 0.8 cm^{-1} is found in AFM state due to different V-V distances. In both magnetic phases, mode-VII is found to be prominent, however, it displays a phonon softening as the magnetic phase is switched to AFM state (206.4 cm^{-1} for FM and 203.2–202.4 cm^{-1} for AFM state). Both the phonon shift and the phonon splittings can be observed in a Raman measurement in order to distinguish the magnetic state of the structure. In contrast, the phonon mode-VI is non-degenerate for both magnetic states and it is shown to be prominent only at AFM state. In addition, its frequency hardens from 189.7 cm^{-1} at FM state to 191.1 cm^{-1} at AFM state. Apparently, the change in the frequency of in-plane mode (mode-VII) is more significant than mode-VI due to the variation of V-V distance between two magnetic phases.

Another distinctive feature of Raman spectra can be seen for the modes labeled as IV and V. In both of the phonon modes, the vibrations are dominated by I atoms while V atoms have negligible contribution. The relative frequency shift of the two modes is found to be 20.6 and 16.2 cm^{-1} for FM and AFM states, respectively which is significant for their observation in a Raman measurement. In addition, the Raman activity ratio of mode-IV to that of mode-V is much greater for AFM state. In the low-frequency regime (<100 cm^{-1}), there are three prominent peaks labeled as I, II, and III. The modes I and III are attributed to the coupled in-plane and out-plane vibrations of I atoms while V atoms have small in-plane vibrations against each other. In contrast, in mode II only I atoms have coupled motion. The frequency of mode I is found to be 47.3 cm^{-1} at FM and 45.3 cm^{-1} at AFM states that the frequency difference is still observable. Moreover, the relative frequencies of the modes II and III are calculated to be 7.4 and 8.3 cm^{-1} for FM and AFM states, respectively. Apart from the phonon frequencies, the high Raman activities of the modes II and III in AFM state are distinctive features of AFM monolayer VI_3. Overall, the calculated Raman activities and the frequencies of the phonon modes are found to be valuable for the identification of the magnetic state in monolayer VI_3.

The electronic properties of FM and AFM magnetic states in monolayer VI_3 are found to display semiconducting features with relatively different band gaps. As presented in Fig. 1(f) and (g), in the AFM state, monolayer VI_3 exhibits semiconducting behavior with a band gap of 184 meV for both spin components while the FM state is found to possess semiconducting character with band gap of 68 meV for one spin channel. In addition, in FM state the valence band maximum (VBM) and conduction band minimum (CBM) for one spin channel are located at different points in the BZ. The VBM and CBM are located in between the Γ and the M points resulting in an indirect band gap nature. In the case of AFM phase, VBM and CBM reside near the Γ and the K points, respectively in between the Γ-K path. Notably, the two magnetic states of monolayer VI_3 display semiconducting characteristic with 116 meV difference between their energy band gaps which may be useful for optically distinguishing the magnetic state of the structure.

In a recent experimental study concerning 2D form of VI_3, it was reported that holes in the center of honeycomb networks of V atoms have tendency to be occupied by excessive V atoms [31]. In order to clarify the effect of excessive V atoms on the properties of monolayer VI_3, 1/16, 1/9, 1/4, and fully-doped VI_3 structures are formed (see Fig. 2(a), (b), (e), and (f)). Depending on the dopant level in monolayer VI_3, the atomic bond distances between V-I and V-V are found to vary

due to structural changes.

As shown in Fig. 2, FM ground state of VI_3 is robust in partially-doped VI_3 structures, however, AFM state is found to be more favorable as the monolayer VI_3 is fully-doped. The structural transition from VI_3 to VI_2 has a significant effect on the magnetic ground state of the structure. The electronic band dispersions for each doped-VI_3 structures are presented in Fig. 2(c), (d), (g), and (h). For the low dopant concentrations, i.e. for 1/16 and 1/9, structure exhibits half-metallic behavior in its ground state. As shown in Fig. 2(c) and (d), the direct and indirect energy band gaps for the semiconducting spin channels are calculated to be 1.98 and 1.92 eV for 1/16 and 1/9 doping levels, respectively. As the doping concentration increases to 1/4, structure turns into a semiconductor for both spin-channels (see Fig. 2(g)). The calculated band gaps are 0.34 and 2.01 eV for different spin components. In addition, the global band gap, 0.34 eV, is found to possess indirect nature. In the case of fully-doped structure (monolayer VI_2), the electronic bands are degenerate due to AFM ground state and the structure is an indirect band gap semiconductor with a band gap of 1.16 eV. It is seen that electronically monolayer VI_3 is found to exhibit semiconducting behavior at least for one spin-channel for different doping levels. In addition, the electronic band gap tunability via V doping (in a wide range of 0.34–1.98 eV) of monolayer VI_3 increases its importance in optoelectronic device applications.

4. Strain engineering in monolayer VI_3

Strain is a common effect which can occur in 2D materials either naturally or externally as a controllable tool for altering the electronic and magnetic properties of the material [47,48]. In addition, strain was reported to be a useful tool for switching the magnetic state of a material [49,21]. As in the case of doping, application of strain may affect magnetic and electronic properties of the magnetic monolayer materials. Here, the effect of biaxial strain on dynamical, electronic, and magnetic properties of VI_3 are investigated in accordance with V doping.

In the case of pristine, 1/9 doped, and 1/4 doped monolayer VI_3, the total energy differences per atom between FM and AFM states increase as the structures are biaxially stretched (see in Fig. 3(a)), however, magnetic ground state remains as FM except for the pristine monolayer as the structure is biaxially compressed with strain strengths larger than 4%. At 5% of compressive strain, pristine monolayer VI_3 undergoes a FM-to-AFM magnetic phase transition. For the 1/4 and 1/9 doped structures, compressive biaxial strain results in decreasing of the energy difference between two magnetic states. Decreasing energy difference between FM and AFM phases indicates that under adequate compressive strain magnetic phase transition may occur, however, under such compression dynamical stability of doped VI_3 crystal is crucial. On the other hand, for the fully-doped monolayer VI_3, a magnetic phase transition from AFM-to-FM state occurs over 4% of tensile strain which is quite important for the control of magnetic state in doped-VI_3 structures with mechanical strain. In addition, effect of strain on magnetism of V atoms in pristine and doped structures are examined. Pristine, 1/4 and 1/9 doped structures are found to have lower magnetic moment under compressive strain and higher magnetic moment under tensile strain, as it is presented in Fig. 3(b).

In order to investigate the dynamical stability of the structures under applied strain, the phonon band dispersions are calculated for pristine and fully-doped monolayer VI_3, at 5% of compressive and tensile strains and the results are presented in Supplementary Information. The phononic stability is found to be retained in both structures for FM and AFM magnetic states.

The effect of biaxial strain on electronic band dispersions of pristine, 1/9 V doped, 1/4 V doped, and fully-doped monolayer VI_3 are investigated and the results are presented in Fig. 4(a–h). In AFM phase of pristine VI_3 semiconducting behavior is found to be robust for both compressive and tensile strains while in FM phase transforms from

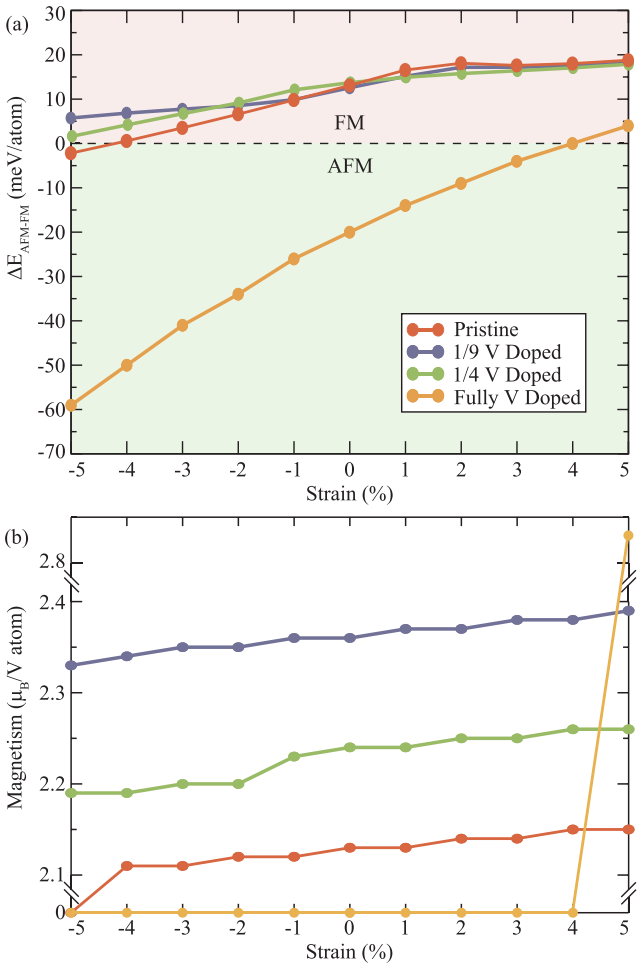

Fig. 3. The effect of biaxial strain on the (a) total energy differences of FM and AFM states in pristine, 1/9 V doped, 1/4 V doped, and fully-doped VI_3. (b) magnetic moment per V atom in pristine, 1/9 V doped, 1/4 V doped, and fully-doped VI_3.

semiconductor to half-metal under compressive strain. Under tensile strain, FM phase of pristine VI_3 retains its semiconducting property. 1/9 V doped VI_3 is found to be semiconductor in its AFM phase at strain-free structure and its band gap increases with increasing compressive strain while it decreases with increasing tensile strain. Importantly, FM 1/9 V doped structure undergoes half-metallic-to-semiconducting behavior with increasing tensile strain. The 1/4 doped monolayer VI_3 is found to display robust metallic nature via applied strain in its AFM state. Moreover, its FM structure exhibits robust semiconducting behavior with varying electronic band gap which increases with increasing tensile strain. However, its electronic band structure at 5% of compressive strain (see Fig. 4(e)) shows that the structure has tendency to possess transition to a metallic state over 5% of compressive strain. In the case of fully-doped monolayer VI_3, the band gap and semiconducting nature of AFM state are preserved while the magnetic state switches to FM over 4% of tensile strain with robust semiconducting behavior. Apparently, partially-doped VI_3 structures display robust magnetic phases under applied biaxial strain while pristine and fully-doped structures undergo magnetic phase transitions with robust semiconducting natures.

5. Conclusions

In this study, the dopant- and strain-dependent structural, magnetic, electronic, and vibrational properties of recently synthesized monolayer VI_3 were investigated in order to clarify the observations in the recent

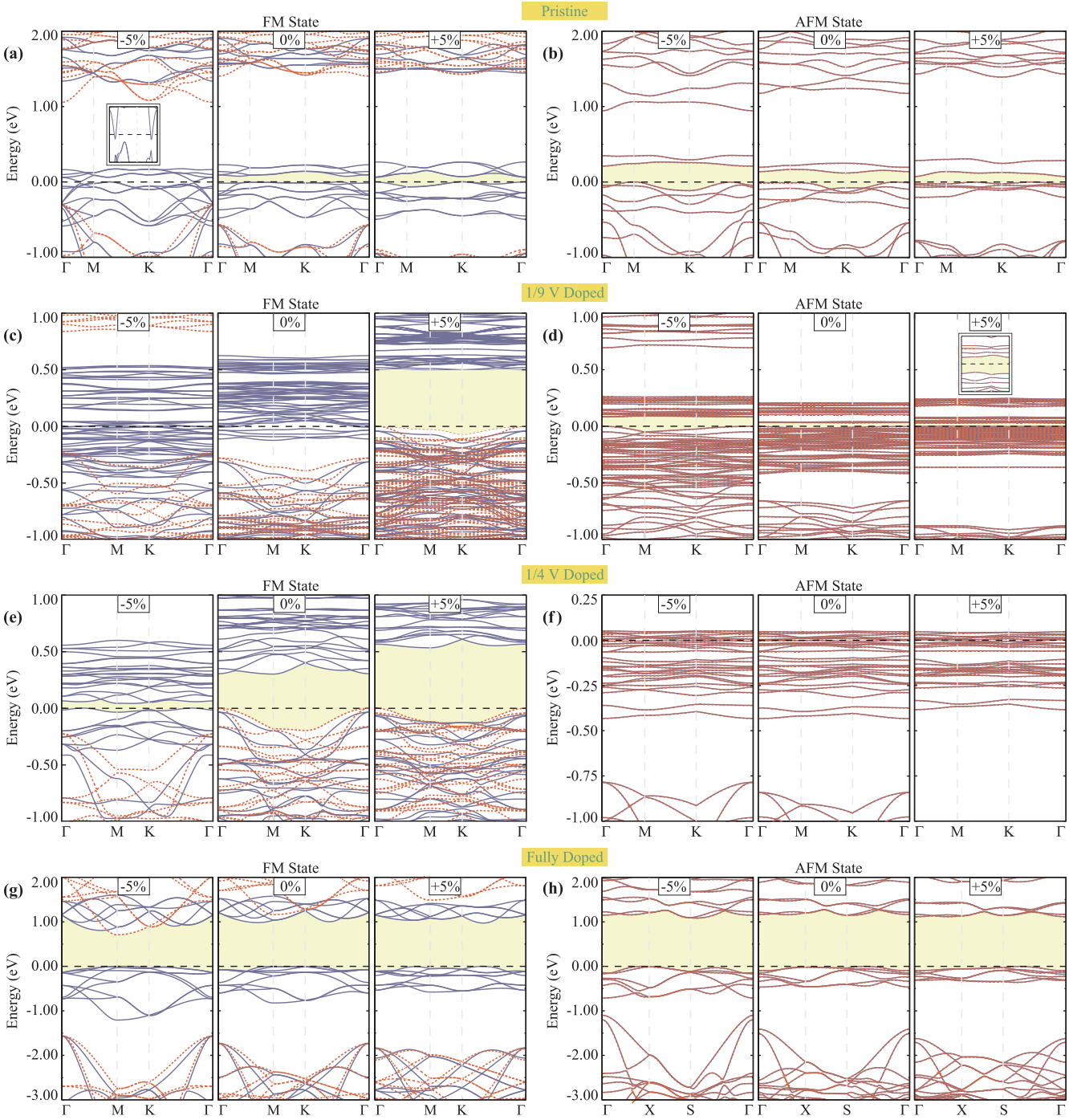

Fig. 4. The strain-dependent electronic band dispersions of monolayer VI_3 for; (a) FM and (b) AFM pristine, (c) FM and (d) AFM 1/9 V doped, (e) FM and (f) AFM 1/4 V doped, (g) FM, and (h) AFM fully-doped structures. The insets show the strain dependent electronic band structures of 5% compressed FM pristine and 5% stretched AFM 1/9 doped VI_3 structures.

experiment. Total energy optimizations indicated that in its dynamically stable structure, monolayer VI_3 possesses FM, semiconducting ground state. The FM and AFM states of VI_3 were found to display distinctive vibrational features in their Raman spectra which is useful for distinguishing the magnetic phase. Our analysis on magnetic and electronic properties of the V-doped VI_3 structures revealed that as monolayer VI_3 is fully-doped by V atoms, it displays a structural phase transition to VI_2 which exhibits AFM semiconducting behavior with a relatively larger band gap in its ground state. Contrarily, for the doping levels in lower concentrations (1/16, 1/9, and 1/4) the FM state remains as the ground state with tunable electronic band gap depending on the doping level. Moreover, it was revealed that both pristine and fully-doped-VI_3 display phononic stability under applied tensile and compressive biaxial strains which is quite important for nanoelastic applications of monolayer VI_3. Notably, pristine and fully-doped VI_3 structures were shown to exhibit magnetic phase transitions under compressive and tensile strains, respectively. Further analysis on strain-dependent electronic band dispersions revealed that pristine and fully-doped VI_3 have robust electronic properties while partially-doped structures exhibit robust magnetic states with varying electronic properties.

Declaration of Competing Interest

None.

Acknowledgments

Computational resources were provided by TUBITAK ULAKBIM, High Performance and Grid Computing Center (TR-Grid e-Infrastructure). H.S. Acknowledges financial support from the TUBITAK under the project number 117F095. H.S. acknowledges support from Turkish Academy of Sciences under the GEBIP program. This work is supported by the Flemish Science Foundation (FWO-Vl) by a post-doctoral fellowship (M.Y.).

Appendix A. Supplementary material

Supplementary data associated with this article can be found, in the online version, at https://doi.org/10.1016/j.apsusc.2019.144937.

References

[1] K.S. Novoselov, A.K. Geim, S.V. Morozov, D. Jiang, Y. Zhang, S.V. Dubonos, I.V. Grigorieva, A.A. Firsov, Science 306 (2004) 666.
[2] M. Golor, S. Wessel, M.J. Schmidt, Phys. Rev. Lett. 112 (2014) 046601.
[3] T. Wassman, A.P. Seitsonen, A.M. Saitta, M. Lazzeri, F. Mauri, Phys. Rev. Lett. 101 (2008) 096402.
[4] J. Zhang, J.M. Soon, K.P. Loh, J. Yin, J. Ding, M.B. Sullivian, P. Wu, Nano Lett. 7 (2007) 2370.
[5] A.V. Krasheninnikov, P.O. Lehtinen, A.S. Foster, P. Pyykk, R.M. Nieminen, Phys. Rev. Lett. 102 (2009) 126807.
[6] O.V. Yazyev, L. Helm, Phys. Rev. B 75 (2007) 125408.
[7] M.M. Ugeda, I. Brihuega, F. Guinea, J.M.G. Rodriguez, Phys. Rev. Lett. 104 (2010) 096804.
[8] L.J. de Jongh, J. Appl. Phys. 49 (1978) 1305.
[9] D. Mauri, H.C. Siegmann, P.S. Bagus, E. Kay, J. Appl. Phys. 62 (1987) 3047.
[10] L.J.de. Jongh, Magnetic Properties of Layered Transition Metal Compounds, (Kluwer Academic, Dordrecht, 1990.
[11] N. Samarth, Nature 546 (2017) 216.
[12] M. Gibertini, M. Koperski, A.F. Morpurgo, K.S. Novoselov, Nat. Nanotechnol. 14 (2019) 408.
[13] M.A. McGuire, H. Dixit, V.R. Cooper, B.C. Sales, Chem. Mater. 10 (2014) 1021.
[14] B. Huang, G. Clark, E. Navarro-Moratalla, D.R. Klein, R. Cheng, K.L. Seyler, D. Zhong, E. Schmidgall, M.A. McGuire, D.H. Cobden, W. Yao, D. Xiao, P. Jarillo-Herrero, X. Xu, Nature 546 (2017) 270.
[15] W. Xing, Y. Chen, P.M. Odenthal, X. Zhang, W. Yuan, T. Su, Q. Song, T. Wang, J. Zhong, S. Jia, X.C. Xie, Y. Li, W. Han, 2D Mater. 4 (2017) 024009.
[16] C. Gong, X. Zhang, Science 363 (2019) 706.
[17] S. Jiang, J. Shan, K.F. Mak, Nat. Mater. 17 (2018) 406.
[18] B. Huang, G. Clark, D.R. Klein, D. MacNeill, E. Navarro-Moratalla, K.L. Seyler, N. Wilson, M.A. McGuire, D.H. Cobden, D. Xiao, W. Yao, P. Jarillo-Herrero, X. Xu, Nat. Nanotechnol. 13 (2018) 544.
[19] S. Jiang, L. Li, Z. Wang, K.F. Mak, J. Shan, Nat. Nanotechnol. 13 (2018) 549.
[20] S. Sarikurt, T. Kadioglu, F. Ersan, E. Vatansever, O.U. Akturk, Y. Yuksel, U. Akinci, E. Akturk, Phys. Chem. Chem. Phys. 20 (2018) 997.
[21] F. Iyikanat, M. Yagmurcukardes, R.T. Senger, H. Sahin, J. Mater. Chem. C 6 (2018) 2019.
[22] M. Bonilla, S. Kolekar, Y. Ma, H.C. Diaz, V. Kalappattil, R. Das, T. Eggers, H.R. Gutierrez, M.H. Pha, M. Batzill, Nat. Nanotechnol. 13 (2018) 289.
[23] P.M. Coelho, K.N. Cong, M. Bonilla, S. Kolkar, M.H. Phan, J. Avila, M.C. Asensio, I.I. Oleynik, M. Batzill, J. Phys. Chem. C 123 (2019) 14089.
[24] I. Eren, F. Iyikanat, H. Sahin, Phys. Chem. Chem. Phys. 21 (2019) 16718.
[25] E. Torun, H. Sahin, S.K. Singh, F.M. Peeters, Appl. Phys. Lett. 106 (2015) 192404.
[26] J. He, S. Ma, P. Lyu, P. Nachtigall, J. Mater. Chem. C. 4 (2016) 2518.
[27] K.O. Berry, R.R. Smardzewski, R.E. Mccarley, Inorg. Chem. 8 (1969) 1994.
[28] D. Juza, D. Giegling, H. Schafer, Z. Anorg, Allg. Chem. 366 (1969) 121.
[29] S. Tian, J.F. Zhang, C. Li, T. Ying, S. Li, X. Zhang, K. Liu, H. Lei, J. Am. Chem. Soc. 141 (2019) 5326.
[30] S. Son, M.J. Coak, N. Lee, J. Kim, T.Y. Kim, H. Hamidov, H. Cho, C. Liu, D.M. Jarvis, P.A.C. Brown, J.H. Kim, C.H. Park, D.I. Khomskii, S.S. Saxena, J.G. Park, Phys. Rev. B 99 (2019) 041402.
[31] T. Kong, K. Stolze, E.I. Timmons, J. Tao, D. Ni, S. Guo, Z. Yang, R. Prozorov, R.J. Cava, Adv. Mater. 31 (2019) 1808074.
[32] F. Iyikanat, H. Sahin, R.T. Senger, F.M. Peeters, J. Phys. Chem. C 119 (2015) 10709.
[33] E. Torun, H. Sahin, S. Cahangirov, A. Rubio, F.M. Peeters, J. Appl. Phys. 119 (2016) 074307.
[34] G. Kresse, J. Hafner, Phys. Rev. B. 47 (1993) 558.
[35] G. Kresse, J. Furthmüller, Phys. Rev. B 54 (1996) 11169.
[36] P. Blöchl, Phys. Rev. B 50 (1994) 17953.
[37] J.P. Perdew, K. Burke, M. Ernzerhof, Phys. Rev. Lett. 77 (1996) 3865.
[38] S. Grimme, S. Ehrlich, L. Goerigk, J. Comput. Chem. 32 (2011) 1456.
[39] G. Henkelman, A. Arnaldsson, H. Jónsson, Comput. Mater. Sci. 36 (2006) 354.
[40] D. Alfé, Comput. Phys. Commun. 180 (2009) 2622.
[41] A. Togo, F. Oba, I. Tanaka, Phys. Rev. B 78 (2008) 134106.
[42] A. Fonari, S. Stauffer, <https://github.com/raman-sc/VASP/>, 2013.
[43] M. Yagmurcukardes, F.M. Peeters, H. Sahin, Phys. Rev. B 98 (2018) 085431.
[44] S. Baidya, J. Yu, C.H. Kim, Phys. Rev. B 98 (2018) 155148.
[45] L. Ren, Q. Liu, P. Xu, Z. Zhong, L. Yang, Z. Yuan, K. Xia, Phys. Rev. Appl. 11 (2019) 054042.
[46] L. Webster, J.A. Yan, Phys. Rev. B 98 (2018) 144411.
[47] M. Yagmurcukardes, C. Bacaksiz, E. Unsal, B. Akbali, R.T. Senger, H. Sahin, Phys. Rev. B 97 (2018) 115427.
[48] E. Torun, H. Sahin, S. Cahangirov, A. Rubio, F.M. Peeters, J. Appl. Phys. 119 (2016) 074307.
[49] Y. Ma, Y. Dai, M. Guo, C. Niu, Y. Zhu, B. Huang, ACS Nano 6 (2012) 1695.